Composition and structure of photosystem I in the moss Physcomitrella patens

Busch, Andreas; Petersen, Jorgen; Webber-Birungi, Mariam T.; Powikrowska, Marta; Lassen, Laerke Marie Munter; Naumann-Busch, Bianca; Nielsen, Agnieszka Zygadlo; Ye, Juanying; Boekema, Egbert J.; Jensen, Ole Norregaard

Published in:
Journal of Experimental Botany

DOI:
10.1093/jxb/ert126

Publication date:
2013

Journal of Experimental Botany, Vol. 64, No. 10, pp. 2689–2699, 2013
doi:10.1093/jxb/ert126 Advance Access publication 16 May, 2013
This paper is available online free of all access charges (see http://jxb.oxfordjournals.org/open_access.html for further details)

Journal of Experimental Botany
www.jxb.oxfordjournals.org

RESEARCH PAPER

Composition and structure of photosystem I in the moss *Physcomitrella patens*

Andreas Busch[1], Jørgen Petersen[2], Mariam T. Webber-Birungi[3], Marta Powikrowska[1], Lærke Marie Münter Lassen[1], Bianca Naumann-Busch[1], Agnieszka Zygadlo Nielsen[1], Juanying Ye[2], Egbert J. Boekema[3], Ole Nørregaard Jensen[2], Christina Lunde[1] and Poul Erik Jensen[1]*

[1] VKR Research Centre 'Pro-Active Plants' and Center for Synthetic Biology, Department of Plant and Environmental Sciences, University of Copenhagen, Thorvaldsensvej 40, 1871 Frederiksberg C, Denmark
[2] Department of Biochemistry and Molecular Biology, University of Southern Denmark, Odense, Denmark
[3] Electron Microscopy Group, Groningen Biomolecular Sciences and Biotechnology Institute, University of Groningen, Nijenborgh 7, 9747 AG Groningen, The Netherlands

*To whom correspondence should be addressed. Email: peje@life.ku.dk

Received 19 November 2012; Revised 27 February 2013; Accepted 8 April 2013

Abstract

Recently, bryophytes, which diverged from the ancestor of seed plants more than 400 million years ago, came into focus in photosynthesis research as they can provide valuable insights into the evolution of photosynthetic complexes during the adaptation to terrestrial life. This study isolated intact photosystem I (PSI) with its associated light-harvesting complex (LHCI) from the moss *Physcomitrella patens* and characterized its structure, polypeptide composition, and light-harvesting function using electron microscopy, mass spectrometry, biochemical, and physiological methods. It became evident that *Physcomitrella* possesses a strikingly high number of isoforms for the different PSI core subunits as well as LHCI proteins. It was demonstrated that all these different subunit isoforms are expressed at the protein level and are incorporated into functional PSI–LHCI complexes. Furthermore, in contrast to previous reports, it was demonstrated that *Physcomitrella* assembles a light-harvesting complex consisting of four light-harvesting proteins forming a higher-plant-like PSI superstructure.

Key words: Photosystem I, photosynthesis, *Physcomitrella patens*, moss, state transitions, structure.

Introduction

Photosystem I (PSI) catalyses the light-driven electron transport from plastocyanin in the thylakoid lumen to $NADP^+$ in the stroma. It is composed of a core complex responsible for charge separation and the first steps of electron transport and a peripheral antenna system, which are involved in light harvesting and transfer of excitation energy to the reaction centre (Jensen *et al.*, 2007; Busch and Hippler, 2011). In plants, PSI is a monomer consisting of at least 16 different proteins to which four peripheral light-harvesting proteins (Lhca1–Lhca4) are attached in a crescent at the PsaF/PsaJ side of the core complex (Amunts and Nelson, 2009).

Throughout the evolution of cyanobacteria towards higher plants, the reaction centre has remained largely conserved with changes only in regard to a few small peripheral subunits. While the subunit PsaX is only present in thermophilic cyanobacteria and PsaM in cyanobacterial and red algal PSI, they are absent in higher plants (Vanselow *et al.*, 2009). In contrast, subunits like PsaG, -H, -N, and -O are acquired in order to accommodate the main structural changes from a trimeric to a monomeric PSI and the acquisition of an external antenna system (Amunts and Nelson, 2009). The extrinsic PSI antenna system is more variable, reflecting the different

Abbreviations: cyt_{c6}, Cytochrome c6; EST, expressed sequence tag; LC, liquid chromatography; LHC, light-harvesting complex; MS, mass spectrometry; PS, photosystem.

environmental conditions that photosynthetic organisms thrive in. While the higher plant crystal structure only shows four different light-harvesting proteins associated with PSI (Ben-Shem *et al.*, 2003), two additional Lhca proteins—Lhca5 and Lhca6—have been identified in *Arabidopsis thaliana* (hereafter *Arabidopsis*) (Jansson, 1999). However, both are expressed only at a very low level (Klimmek *et al.*, 2006), and solid biochemical data only exist for Lhca5, which has been shown to bind to PSI in substoichiometric amounts in *Arabidopsis* (Ganeteg *et al.*, 2004). Recently, Lhca5 and Lhca6 have been implicated in NAD(P)H dehydrogenase–PSI supercomplex formation, which is involved in cyclic electron transfer (Peng and Shikanai, 2011).

Research on the structure and function of PSI so far has focused mainly on cyanobacteria, algae (diatoms and green and red algae) and higher plants. Only recently have bryophytes (mosses, liverworts and hornworts), which diverged from the ancestor of seed plants more than 400 million years ago (Falkowski, 2006), come into focus as they represent the transition from aquatic to terrestrial life. Analysing the structure and function of the photosynthetic machinery in a moss such as *Physcomitrella patens* (hereafter *Physcomitrella*) can provide valuable insights into the evolution of the system during the adaptation to a terrestrial environment. Together with its evolutionary position, its remarkable resistance against various abiotic stresses such as salt, drought, osmotic stress, and UV radiation have made the moss *Physcomitrella* an interesting model organism to identify new stress-tolerance genes (Frank *et al.*, 2005; Wolf *et al.*, 2010).

The evolutionary intermediate position of *Physcomitrella* is clearly reflected within the photosynthetic machinery and was demonstrated recently with the analysis of the non-photochemical quenching mechanism in this moss (Alboresi *et al.*, 2010; Gerotto *et al.*, 2011). Excess absorbed light energy is dissipated thermally, which regulated by an ancient light-harvesting protein (LhcSR) in green algae (Peers *et al.*, 2009). However, during evolution towards higher plants, this protein got lost and was functionally replaced by the PsbS protein (Koziol *et al.*, 2007). As *Physcomitrella* possesses both proteins (LhcSR and PsbS), it is evident that *Physcomitrella* represents an intermediate between algae, which employ LhcSR proteins for photoprotection, and higher plants, which rely on the function of PSBS and have lost the LhcSR genes.

Previous analysis of *Physcomitrellas* photosynthetic machinery focused on the antenna system and their photoprotective mechanisms (Alboresi *et al.*, 2010; Gerotto *et al.*, 2011). Interestingly, a considerably higher number of chlorophyll *a*/*b*-binding (Cab) proteins in *Physcomitrella* compared with *Arabidopsis* were identified in a bioinformatics study (Alboresi *et al.*, 2008), which confirmed earlier studies by Hofmann *et al.* (1999). Surprisingly, it was found that an orthologue of Lhca4 was absent in *Physcomitrella*, which resulted in a PSI–light-harvesting complex I (LHCI) complex with a blue-shifted 77K fluorescence emission spectra due to the lack of the red chlorophyll bound to Lhca4 (Alboresi *et al.*, 2008). Based on results obtained from native gel electrophoresis, it was consequently proposed that *Physcomitrella* possesses a smaller PSI–LHCI complex compared to *Arabidopsis* (Alboresi *et al.*, 2008). However, to date, no further evidence for this assumption has been provided. In this report, we have provided a detailed study of the entire PSI–LHCI complex of *Physcomitrella* including the composition of the core complex. For this, we undertook careful preparation of thylakoids and pigment–protein complexes, which we analysed using mass spectrometry, spectroscopic methods, single-particle electron microscopy imaging, and biochemical assays to provide a comprehensive characterization of the PSI–LHCI structure, composition, and function.

Materials and methods

Plant material and growth conditions

Physcomitrella patens (Hedw.) ecotype Grandsen (Ashton and Cove, 1977) was grown at 22 °C on cellophane discs placed on solid minimal medium (Ashton *et al.*, 1979), supplemented with 0.5 g l^{-1} of ammonium tartrate. Standard irradiance conditions were 50 µmol photons m^{-2} s^{-1} white light for 16 h and darkness for 8 h. Cultures were overlaid with filter foil to shift into state 1 (filter 27, medium red, >600 nm, preferentially exciting PSI; Lee Filters, Hampshire, UK) or state 2 (filter 183, moonlight blue, <550 nm, preferentially exciting PSII, Lee Filters)

Preparation of thylakoid membranes and isolation of PSI

Protonemata (10–14 d old) was harvested, flash frozen in liquid nitrogen and stored at –80 °C until further use. Crude thylakoids were isolated as described by Haldrup *et al.* (1999). Protonemal tissue was disrupted in homogenization buffer using a homogenizer (Kinematica Brinkman Polytron PT3000) or a pre-chilled mortar and pestle. Further clean-up of thylakoids followed a modified protocol of Chua and Bennoun (1975). Thylakoids were resuspended in 12 ml H3 [1.8 M sucrose, 5 mM Tricine (pH 7.5), 10 mM EDTA], which was overlaid by 12 ml H4 [1.3 M sucrose, 5 mM Tricine (pH 7.5), 10 mM EDTA] and 12 ml H5 [0.5 M sucrose, 5 mM Tricine (pH 7.5), 10 mM EDTA]. After centrifugation (SW28 rotor, 24000 rpm, 1 h, 4 °C), the thylakoids accumulated at the H3/H4 interphase. The thylakoids were collected, diluted with 5 mM Tricine (pH 7.5) and pelleted (20 000*g*, 4 °C, 10 min). The resulting pellet was resuspended in a small volume of homogenization buffer without ascorbate and BSA but with 20% glycerol (v/v) and stored at –80°C. For analysis of the phosphorylation status of thylakoids, all buffers were supplemented with 10 mM NaF and 1 mM Na_3VO_4.

PSI was isolated according to the method of Mullet *et al.* (1980) with some modifications. The thylakoids were resuspended in solubilization buffer [20 mM Tricine (pH 7.5), 10 mM EDTA, 0.7% β-D-dodecyl-maltoside] to a final chlorophyll concentration of 0.8 µg $µl^{-1}$. The samples were incubated on ice for 15 min with occasional gentle mixing. After centrifugation (5 min, 16 000*g*, 4 °C), the supernatant was loaded onto a linear sucrose gradient [0.4–0.85 M sucrose, 20 mM Tricine (pH 7.5), 0.06% β-D-dodecyl-maltoside]. After centrifugation (SW41Ti rotor, 34 000 rpm, 16–18 h, 4 °C), the PSI was retrieved with a syringe and stored at –80°C. Total chlorophyll was determined in 80% acetone according to the method of Lichtenthaler (1987).

Immunoblot analysis

Criterion XT 12% Bis-Tris gels and MES buffer (Bio-Rad Laboratories, Hercules, CA, USA) were used to separate the proteins and followed by transferring the electrophoresed proteins to nitrocellulose membranes. After immunoblotting, the antibodies were detected using a chemiluminescent detection system (SuperSignal®; Thermo Scientific, Rockford, USA) according to

the instructions of the manufacturer. The chemiluminescent signal produced was recorded digitally using a cooled CCD camera with the AC1 AutoChemi System (Ultra-Violet Products, Cambridge, UK) and analysed using LabWorks Analysis software (Ultra-Violet Products). Antibodies against Lhca1–Lhca4 were obtained from Agrisera (Uppsala, Sweden). Anti-phosphothreonine antibodies were obtained from Cell Signaling Technology (MA, USA).

State transition measurements

Photosynthetic state transitions were measured using a DUAL-PAM-100 (Walz; Effeltrich, Germany). After 45 min dark adaptation, a saturating flash was applied. Subsequently, samples were illuminated for 20 min with the built-in blue light at 44 μE m^{-2} s^{-1}, followed by a saturating flash to obtain Fm2. The light was switched to built-in far-red light with an intensity of 51 μE m^{-2} s^{-1}. After 20 min of far-red light, a saturating flash was applied to obtain Fm1. State transition was calculated using the equation: (Fm1 – Fm2)/Fm1 (Jensen *et al.*, 2000).

Mass spectrometry

Proteins were separated on a pre-cast NuPAGE® Bis-Tris gel. In-gel-fixed proteins were visualized using colloidal Coomassie blue staining. Protein bands were excised from the gel. Cysteines were reduced and *S*-alkylated prior to in-gel trypsin digestion, peptide extraction, and analysis by liquid chromatography-tandem mass spectrometry (LC-MS/MS) (Jensen *et al.*, 1998). Mass spectra were acquired in positive-ion mode applying an automatic data-dependent switch between one Orbitrap survey MS scan in the mass range of 300–1650 *m/z* followed by fragmentation and detection of the seven most intense ions observed from the MS scan. The target value in the Orbitrap for the MS scan was 1 000 000 ions at a resolution of 50 000 at *m/z* 400, with a higher-energy collisional dissociation-normalized collision energy of 40. The ion selection threshold was set to 15 000 counts. The Orbitrap was coupled to a ThermoFisher/Proxeon EasyLC system. Solvent A was 0.1% formic acid in water and solvent B was 0.1% formic acid in acetonitrile. Peptides were trapped on a homemade 1 cm C18, 150 μm internal-diameter column (ReproSil Pur C18 AQ 3 μm sorbent) and separated on a homemade 15 cm, 75 μm internal-diameter C18 analytical column (particle size 3 μm). The run time was 113 min per sample. Raw files were processed and searched using Proteome Discoverer version 1.3.0.339 (Thermo Fisher Scientific, Bremen, Germany). Tandem mass spectra were converted to peak lists and searched against a *Physcomitrella* protein sequence database (https://www.cosmoss.org/physcome_project/wiki/Genome_Annotation/V1.6). Database searches were performed with the following parameters: precursor mass tolerance at 10 ppm and MS/MS mass tolerance at 0.1 Da. Variable modifications included methionine oxidation and deamidation of asparagine and glutamine. Carbamidomethylation on cysteine was set as a fixed modification.

Analysis of Physcomitrella *PSI complex by single-particle electron microscopy*

Samples from the sucrose gradient were dialysed (12–14 kDa molecular weigh cut-off) against buffer [5 mM Tricine (pH 7.8), 5 mM $MgCl_2$, 0.03% β-D-dodecyl-maltoside) overnight to reduce the sucrose content and thus improve the contrast in the electron microscope. Samples were then stained with 2% uranyl acetate on glow-discharged carbon-coated copper grids. Electron microscopy was performed on a Philips CM120 electron microscope equipped with a LaB6 filament operating at 120 kV. Images (2048 × 2048 pixels) were recorded with a Gatan 4000 SP 4 K slow-scan CCD camera at 130 000× magnification at a pixel size (after binning the images) of 2.3 Å at the specimen level with GRACE software for semi-automated specimen selection and data acquisition (Oostergetel *et al.*, 1998). Single-particle analysis was performed using GRIP software including multireference and non-reference alignments, multivariate statistical analysis, and classification, as described by Boekema *et al.* (1999).

$NADP^+$ photoreduction

The $NADP^+$ photoreduction activities of thylakoids from *Arabidopsis* and *Physcomitrella* were determined as described by Jensen *et al.* (2011).

The total P700 content was determined as described by Markwell *et al.* (1980) from the ferricyanide-oxidized minus ascorbate-reduced difference spectrum using an extinction coefficient of 64 000 M^{-1} cm^{-1} at 700 nm (Hiyama and Ke, 1972; Sonoike and Katoh, 1988). The thylakoids were solubilized in 0.2% Triton X-100, and the measurements were repeated four to five times on several independent thylakoid preparations.

Results

Photosynthetic genes in Physcomitrella *are highly redundant*

To elucidate the number of genes encoding PSI subunits in the genome of *Physcomitrella*, the entire set of *Arabidopsis* PSI genes was taken from Jensen *et al.* (2007) and used as reference for a BLAST search on the most current moss genomic database (version 1.6; see Methods). To avoid ambiguities during the BLAST search, the putative chloroplast signal sequence was determined using ChloroP (Emanuelsson *et al.*, 1999) and the signal sequence was removed from the *Arabidopsis* reference sequences before the search was performed. To our surprise, *Physcomitrella* contained a large number of isoforms for the different PSI subunits (Table 1). For the chloroplast-encoded subunits PsaA, -B, -C, -I, and –J, only one copy was found in the chloroplast genome; however, the nuclear-encoded subunits showed a large number of isoforms ranging from two copies of PsaG, -H, and -O up to four different gene entries for PsaD and PsaF. Additionally, we assessed the number of available moss expressed sequence tags (ESTs) moss genomic database (version 1.6) for each of the nuclear-encoded gene copies, assuming that the number of available ESTs indicates a relative expression level of the respective genes. In addition to the total number of ESTs, we also assessed their number in the different tissue types: protonema, gametophore, and sporophyte (Table 1). To obtain a consistent nomenclature, we ranked the isoforms according to their number of ESTs and numbered them starting with the isoform with the highest number of ESTs.

EST support could be found for almost all nuclear-encoded genes with the exception of *PpPsaK-3* (Pp1s5_396V6.1). However, it became clear that the apparent expression levels differed for the different isoforms of a protein. While, for example, *PpPsaD-4* (Pp1s107_188V6.1) had only 12 ESTs, the *PpPsaD-1* (Pp1s4_321V6.1) isoform was heavily supported by 190 ESTs, indicating that this might be the major PsaD isoform. For the other PSI subunits, it was also evident that at least one isoform appeared to be the dominating form with at least a two-fold higher number of ESTs compared with the other isoforms. With respect to the different tissue types, most of the EST support stemmed from protonemal

Table 1. Identification of PSI–LHCI subunits in *Physcomitrella*. The protein names are indicated, together with where the proteins are encoded [chloroplast (C) or nucleus (N)], the gene copy number in *Arabidopsis*, the hits found by BLAST analysis in moss, a proposed gene designation in moss, and the total number of ESTs found for each gene with the numbers found for the different tissue types indicated in parentheses (protonema+gametophore+sporophyte). Proteins that were identified (+) or not (–) by MS are indicated. NA, not applicable.

Protein	Encoded in:	No. copies in *Arabidopsis*	BLAST hits in *Physcomitrella*	Proposed designation	No. ESTs	Identified with MS/MS
Core proteins						
PsaA	C	1	PhpapaCp039	PpPsaA	NA	+
PsaB	C	1	PhpapaCp040	PpPsaB	NA	+
PsaC	C	1	PhpapaCp076	PpPsaC	NA	+
PsaD	N	2	Pp1s4_321V6.1	PpPsaD-1	190 (177+4+9)	+
			Pp1s77_69V6.1	PpPsaD-2	102 (88+7+7)	+
			Pp1s1_788V6.1	PpPsaD-3	90 (80+6+4)	+[a]
			Pp1s107_188V6.1	PpPsaD-4	12 (8+4+0)	–
PsaE	N	2	Pp1s334_17V6.1	PpPsaE-1	60 (60+0+0)	+
			Pp1s319_36V6.1	PpPsaE-2	53 (51+0+2)	+
			Pp1s101_2V6.1	PpPsaE-3	37 (33+2+2)	+
PsaF	N	1	Pp1s19_276V6.1	PpPsaF-1	223 (203+11+9)	–
			Pp1s345_25V6.1	PpPsaF-2	150 (139+3+8)	+
			Pp1s121_54V6.1	PpPsaF-3	108 (70+36+2)	+
			Pp1s80_23V6.1	PpPsaF-4	37 (33+3+1)	–
PsaG	N	1	Pp1s83_246V6.1	PpPsaG-1	183 (138+18+27)	+
			Pp1s78_205V6.1	PpPsaG-2	18 (18+0+0)	+
PsaH	N	2	Pp1s89_62V6.1	PpPsaH-1	42 (26+2+14)	+
			Pp1s206_11V6.1	PpPsaH-2	20 (14+2+4)	+
PsaI	C	1	PhpapaCp029	PpPsaI	NA	–
PsaJ	C	1	PhpapaCp017	PpPsaJ	NA	–
PsaK	N	1	Pp1s74_135V6.1	PpPsaK-1	72 (66+2+4)	–
			Pp1s5_384V6.1	PpPsaK-2	27 (19+4+4)	–
			Pp1s5_396V6.1	PpPsaK-3	0	–
PsaL	N	1	Pp1s54_165V6.1	PpPsaL-1	201 (153+22+26)	+
			Pp1s15_408V6.1	PpPsaL-2	75 (69+1+5)	–
			Pp1s41_267V6.1	PpPsaL-3	71 (66+4+1)	–
PsaM	C	0	PhpapaCp051	PpPsaM	NA	–
PsaN	–	1	–	–	–	–
PsaO	N	1	Pp1s248_60V6.1	PpPsaO-1	111 (100+3+8)	–
			Pp1s248_61V6.1	PpPsaO-2	49 (48+1+0)	+
Light-harvesting proteins*						
Lhca1			Pp1s158_109V6.1	Lhca1.1		+
			Pp1s161_32V6.1	Lhca1.2		+
			Pp1s247_7V6.1	Lhca1.3		+
Lhca2			Pp1s32_1V6.1	Lhca2.1		–
			Pp1s330_37V6.1	Lhca2.2		+
			Pp1s241_66V6.1	Lhca2.3		+
			Pp1s651_2V6.1	Lhca2.4		+
Lhca3			Pp1s214_86V6.1	Lhca3.1		–
			Pp1s429_33V6.2	Lhca3.2		+
			Pp1s197_123V6.1	Lhca3.3		+
			Pp1s214_87V6.1			
Pp1s214_87V6.2	Lhca3.4		–			
Lhca5			Pp1s284_6V6.1	Lhca5		+

[a] Unique peptide that was only identified using version 1.2 of the moss genome database.
* annotation according to Alboresi et al., 2008.

tissue. However, the distribution of abundance within the gametophores and sporophyte followed the number of ESTs in the protonema. One notable exception was *PpPsaF-3* (Pp1s121_54V6.1), which was only the third most abundant isoform in the protonemal tissue but was the dominating isoform in the gametophore (Table 1). However, this result has to be taken with caution as the sample size of the EST collection was too small for robust quantitative conclusions.

It was of note that the chloroplast genome of *Physcomitrella* also encoded the cyanobacterial PsaM subunit, which is not

present in vascular plants (Table 1). In contrast, no PsaN homologue could be identified in the *Physcomitrella* genome.

Additional thylakoid clean-up is required for efficient biochemical assays

Standard plant protocols for thylakoid isolation (Haldrup *et al.*, 1999) used on *Physcomitrella* gave a weak and noisy signal when functional measurements such as $NADP^+$ photoreduction (Fig. 1A, dotted trace) were performed. Hence, an additional clean-up step was tested to obtain more homogenous thylakoids for proper biochemical assays. We subjected isolated crude thylakoids to an additional sucrose density centrifugation on a discontinuous sucrose gradient according to the method of Chua and Bennoun (1975). After centrifugation, the thylakoids were collected at the 1.8/1.3 M interphase (Fig. 1B), while insoluble components such as starch formed a pellet. Additionally, a white layer could be observed at the 1.3/0.5 M interphase, which probably represents additional membranes such as the plasmalemma, endoplasmic reticulum and/or Golgi. We compared the performance of crude thylakoid extract and purified thylakoids in a $NADP^+$ photoreduction assay using equivalent amounts of chlorophyll (Fig. 1A). It was clear that additional thylakoid purification enhanced the quality of the signal significantly (Fig. 1A, solid trace). Hence, we used sucrose density gradient-purified thylakoids for all subsequent experiments.

Different PSI subunits can be detected by immunoblotting

An extensive collection of plant PSI-subunit specific antibodies has been established (Jensen *et al.*, 2007). In order to elucidate whether these antibodies can be used to study *Physcomitrella* PSI–LHCI complexes, *Physcomitrella* thylakoids and isolated PSI were separated by SDS-PAGE, transferred to a nitrocellulose membrane and probed with the different antibodies (Fig. 2A). Isolated thylakoids of *Arabidopsis* served as a reference for the individual antibodies. It was evident that for subunits PsaA, -C, -D, -F, -H, -K, and -L, bands that corresponded to *Arabidopsis* could be detected both in thylakoids and in PSI complexes of *Physcomitrella*. In contrast, antibodies directed towards the PsaE, -G, -N, and -O subunits gave no detectable signal in either *Physcomitrella* thylakoids or the PSI samples.

Interestingly, for PsaD, two bands possibly representing different isoforms could be detected on the immunoblot (Fig. 2A). This assumption was supported by alignment of the four isoforms of PpPsaD (Supplementary Fig. S1 at *JXB* online), which showed that the isoforms PpPsaD-1 and PpPsaD-2 both had an additional insert of 7 aa (DQKPDAK), making the mature protein approximately 1 kDa larger than the other two isoforms.

Another interesting observation was the band pattern obtained for PpPsaF. While for isolated *Arabidopsis* thylakoids only one band was visible, which corresponded to the predicted size of 17.5 kDa (Jensen *et al.*, 2007), the *Physcomitrella* thylakoids and isolated PSI showed two bands

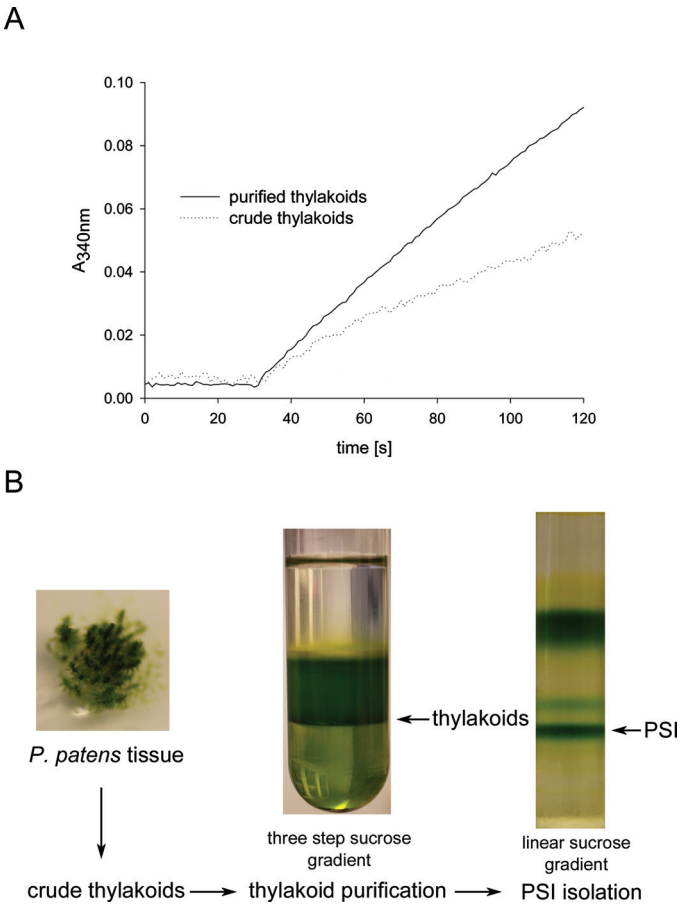

Fig. 1. Isolation of thylakoids from *Physcomitrella*. (A) Absorption trace (at 340 nm) of *in vitro* $NADP^+$ photoreduction assay using crude thylakoids (dotted trace) or purified thylakoids (solid trace) of *Physcomitrella*. (B) *Physcomitrella* tissue was disrupted and a crude thylakoid extract prepared, which was subjected to a further clean-up step via a discontinuous sucrose gradient (1.8, 1.3, and 0.5 M sucrose layered on top of each other). After centrifugation, the thylakoids were collected at the 1.8/1.3 M sucrose interphase. The thylakoids were used for biochemical assays or were solubilized using β-D-dodecyl-maltoside and subjected to a centrifugation on a linear sucrose gradient to obtain intact the PSI–LHCI complex.

(Fig. 2A). The higher band migrated at around 20 kDa and the lower band was slightly higher than the corresponding *Arabidopsis* band. When aligning the PsaF sequences of *Arabidopsis* and *Physcomitrella*, a 7 aa C-terminal extension (NITVSPR) within the *Physcomitrella* sequence was apparent (Supplementary Fig. S2 at *JXB* online). This extension added approximately 0.8 kDa to the protein size, which could explain the slightly lower electrophoretic mobility of *Physcomitrella* PsaF. Interestingly, this extension can also be found in cyanobacteria (*Synechocystis* sp. PCC 6803), red algae (*Galdieria sulphuraria*) and green algae (*Chlamydomonas reinhardtii*) (Supplementary Fig. S2). However, the nature of the second band with higher molecular weight remains unclear.

To study the composition of the PSI-associated light-harvesting complexes, commercially available antibodies

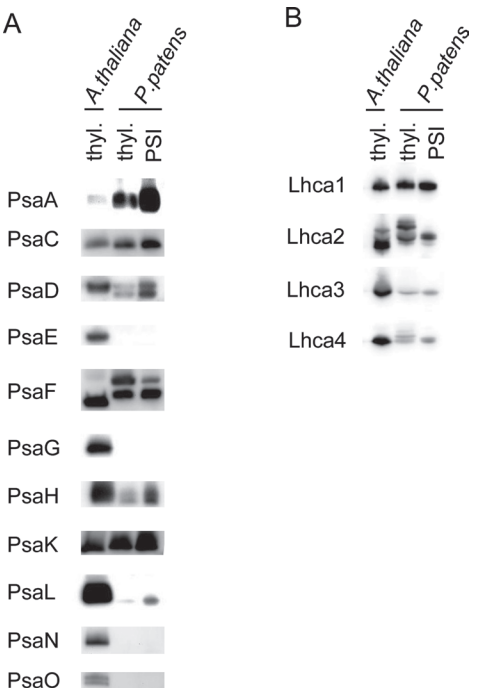

Fig. 2. Immunoblot analysis of PSI subunits in *Physcomitrella*. *Physcomitrella* thylakoids and isolated PSI were separated by SDS-PAGE, blotted, and analysed with the indicated antibodies against different PSI core subunits (A) or light-harvesting proteins (B). *Arabidopsis* thylakoids served as a reference. Samples were loaded according to equal amounts of chlorophyll (5 μg of chlorophyll for thylakoids and 3 μg for isolated PSI).

against Lhca1–4 were likewise used to probe protein blots of thylakoids and PSI isolated from *Physcomitrella* (Fig. 2B). Again, *Arabidopsis* thylakoid proteins served as a reference. Antibodies against Lhca1 and -3 could detect proteins at the size that correspond to the respective sizes of *Arabidopsis* Lhca1 and -3 (Fig. 2B), indicating that the antibodies recognized PpLhca1 and -3. In contrast, the antibody against Lhca2 produced two major bands with the *Physcomitrella* thylakoids, with the lower one running slightly higher than Lhca2 of *Arabidopsis*. Interestingly, the high-molecular-weight band for Lhca2 in *Physcomitrella* was not present in isolated PSI, indicating that it represented non-specific binding of the antibody to proteins present in *Physcomitrella* thylakoids. Again, the Lhca2 band in *Physcomitrella* PSI indicated a slightly larger protein than that in *Arabidopsis*, which is in agreement with the predicted sizes of the mature Lhca2 (*Arabidopsis* ~23.3 kDa, *Physcomitrella* ~24.4 kDa). Surprisingly, Lhca4 gave a signal in the isolated thylakoids and PSI–LHCI of *Physcomitrella* despite the fact that *Physcomitrella* does not encode an Lhca4-like subunit (Alboresi *et al.*, 2008). Hence, the obtained signal most likely stemmed from non-specific binding of the antibody to other Lhc proteins.

Clearly, immunoblot-based analysis of isolated PSI–LHCI from *Physcomitrella* was not able to resolve the existence of all the different isoforms of PSI subunits encoded by *Physcomitrella*. Therefore, the isolated *Physcomitrella* PSI–LHCI complex was characterized further by proteome analysis by MS to resolve its subunit composition in more detail.

Different isoforms are clearly identified at the protein level

For MS analyses, isolated *Physcomitrella* PSI samples were digested with trypsin and separated on an LC system before MS/MS analysis was carried out on an LTQ Orbitrap system. With this approach, we aimed to identify unambiguously the different isoforms for the respective PSI subunits at the protein level. The obtained results clearly showed that the diversity of isoforms for the different PSI subunits encoded by *Physcomitrella* (Table 1) was also reflected at the protein level (Table 1 and Supplementary Table S1 at *JXB* online).

Using MS analysis, we were able to identify the following PSI core subunits: PsaA, -B, -C, -D, -E, -F, -G, -H, -K, -L, and -O (Table 1 and Supplementary Table S1). Only the small subunits PsaI, PsaJ, and PsaM could not be identified unambiguously with unique peptides. This might be due to the fact that these small proteins do not always yield tryptic peptides suitable for MS analysis due to size or charge issues. Alternatively, the peptide sequences that were detected could not be assigned unambiguously because they were not unique.

With respect to the different isoforms of the subunits encoded by *Physcomitrella* (Table 1), we could uniquely identify at least one isoform for each of the PSI core subunits with the exception of PsaK (Table 1 and Supplementary Table S1), while for PsaE (three isoforms), -G (two isoforms), and -H (two isoforms) we could identify all possible isoforms. For PsaD (four isoforms) and PsaO (two isoforms), one isoform remained unidentified, and for PsaF (four isoforms) and PsaL (three isoforms), two isoforms remained unidentified. It is of note that, for PpPsaD-3, a unique peptide could only be identified using version 1.2 of the moss database. Although we could identify three distinct peptides uniquely identifying PsaK (Supplementary Table S1), we were not able to match them to any of the three different isoforms of PsaK, as the peptides were derived from a highly conserved region of PsaK (Supplementary Fig. S3 at *JXB* online and Supplementary Table S1). One peptide uniquely identified PsaK-2, but manual inspection of the fragmented peptide could not rule out other sequence combinations.

With regard to the members of the light-harvesting complex of PSI, we followed the annotation of Alboresi *et al.* (2008). We were able to identify Lhca1, -2, -3, and -5 and most of their different isoforms (Table 1 and Supplementary Table S1). For Lhca1 (three isoforms) and Lhca2 (four isoforms), all isoforms except Lhca2.1 were detected by unique peptides. For Lhca3, two out of four isoforms could be detected, and Lhca5 was present only in one isoform, which also could be identified.

Chl/P700 and in vitro NADP⁺ photoreduction

After characterizing the PSI–LHCI complex at the protein level, we aimed to study the function of *Physcomitrella* PSI further using spectroscopic as well as biochemical methods.

The number of chlorophylls associated with both photosystems but normalized per P700 reaction centre was assessed in thylakoids using chemical oxidation. For *Physcomitrella* thylakoids, we measured 693 ± 66 (n=5) chlorophylls per P700 reaction centre (Table 2), which was only marginally more than the 666 ± 24 chlorophylls per P700 reaction centre that were reported previously for *Arabidopsis* wild-type thylakoids (Jensen *et al.*, 2002).

An *in vitro* $NADP^+$ photoreduction assay was used to measure and assess the activity of *Physcomitrella* PSI. With isolated thylakoids of wild-type *Arabidopsis*, we obtained an activity of 24.35 ± 2.65 μmol s^{-1} per P700 reaction centre of NADPH (n=3; Table 2), which was in good agreement with previously published activities (Jensen *et al.*, 2002). Using the same set-up, we also measured an activity of 11.92 ± 0.85 μmol s^{-1} per P700 reaction centre of NADPH (n=3; Table 2) with isolated *Physcomitrella* thylakoids.

Although in some algae cytochrome can be used as alternative electron donor to PSI when copper becomes a limiting factor (Wood, 1978), higher plants are dependent on the presence of plastocyanin (Weigel *et al.*, 2003). To test the ability of *Physcomitrella* PSI to use cytochrome c6 (cyt_{c6}) as an alternative electron donor, the 2 μM plastocyanin was substituted with 2 μM cyanobacterial cyt_{c6} in the $NADP^+$ photoreduction assay (Table 2). For comparison, we also performed the assay with *Arabidopsis* thylakoids and, as expected, an almost complete loss of activity was recorded. While for *Arabidopsis* thylakoids an activity of 1.61 ± 0 μmol s^{-1} per P700 reaction centre of NADPH (n=3) was recorded, for *Physcomitrella* thylakoids no activity could be seen (0.09 ± 0.12 μmol s^{-1} per P700 reaction centre of NADPH; n=3) (Table 2). Also, a doubling of the cyt_{c6} concentration did not dramatically increase the activity (Table 2). This clearly showed that neither *Arabidopsis* nor *Physcomitrella* PSI is able to utilize cyt_{c6} as an alternative electron acceptor.

State 1–state 2 transitions

We also tested the ability of *Physcomitrella* to induce state transition, the reversible phosphorylation and movement of LHCII to PSI upon overexcitation of PSII (Haldrup *et al.*, 2001). Protonemal tissue was cultivated under blue light (state 2 light) or far-red light (state 1 light) for 1 h. Subsequently, thylakoids were isolated from both states and the phosphorylation pattern of the proteins was analysed by immunoblotting using antibodies against phosphothreonine (Fig. 3). Three major bands at ~40, ~30, and ~25 kDa were visible whose phosphorylation increased under blue light compared with samples derived from far-red light conditions, which was in line with results obtained from thylakoid samples from *Arabidopsis* grown under comparable conditions (Fig. 3). Interestingly, the band at 25 kDa, which represents LHCII proteins (Rintamaki *et al.*, 2000), was not as pronounced in the *Physcomitrella* state 2 conditions as in the *Arabidopsis* state 2, where it represented the strongest band (Fig. 3). This suggested a lower degree of LHCII phosphorylation in *Physcomitrella* compared with *Arabidopsis*. However, these results have to be judged with caution, as the signal intensity is very dependent on the brand of antibody and plant material used (Turkina *et al.*, 2006). The extent of state 1–state 2 transition was additionally assessed by measuring chlorophyll *a* fluorescence on protonema tissue grown on agar plates and compared with intact *Arabidopsis* plants (Supplementary Fig. S4 at *JXB* online). The samples were dark adapted for 45 min and the maximum fluorescence yield was determined. After 20 min of blue light illumination, which favours PSII, the maximum fluorescence in state 2 (Fm2) was determined. Subsequently, the light was changed to far-red light, which favours PSI and induces state 1. Again, after 20 min, the maximum fluorescence (Fm1) was determined. The ability to perform state transitions can be expressed as a ratio of Fm1 and Fm2 [(Fm1 – Fm2)/Fm2], where a smaller ratio indicates a lower state transition (Jensen *et al.*, 2000). For *Physcomitrella*, a ratio of 0.127 ± 0.004 (n=4) was obtained, while for *Arabidopsis* a ratio of 0.167 ± 0.006 (n=3) was measured. These values were significantly different (Student's t-test, P <0.001). Hence, *Physcomitrella* indeed performs state transition; however, it has a slightly smaller capability to do so, in agreement with the lower ability to phosphorylate LHCII (Fig. 3). Additionally, standard photosynthetic parameters were determined (Supplementary Table S2 at *JXB* online).

Table 2. *In vitro* $NADP^+$ photoreduction with different electron donor systems. Values are means ±standard deviation.

	Arabidopsis	***Physcomitrella***
Chlorophyll/P700	666 ± 24[a]	693 ± 66 (n=5)
$NADP^+$ photoreduction (μmol NADPH s^{-1} per P700)		
2 μM plastocyanin	24.35 ± 2.65 (n=3)	11.92 ± 0.85 (n=3)
2 μM cyt_{c6}	1.61 ± 0 (n=3)	0.09 ± 0.12 (n=3)
4 μM cyt_{c6}	3.04 ± 0.31 (n=3)	2.05 ± 0.32 (n=3)

[a] Value taken from Jensen *et al.* (2002).

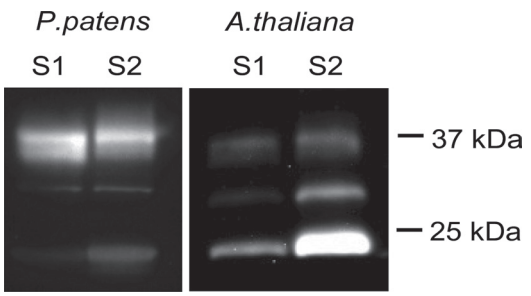

Fig. 3. Analysis of phosphorylation pattern during state transitions. Thylakoids from *Physcomitrella* and *Arabidopsis* under state 1 (S1) and state 2 (S2) conditions were isolated, separated by SDS-PAGE, blotted, and analysed with anti-phosphothreonine antibodies to visualize changes in phosphorylation patterns. The equivalent of 12 and 3 μg of chlorophyll from thylakoids was loaded per lane for *Physcomitrella* and *Arabidopsis*, respectively.

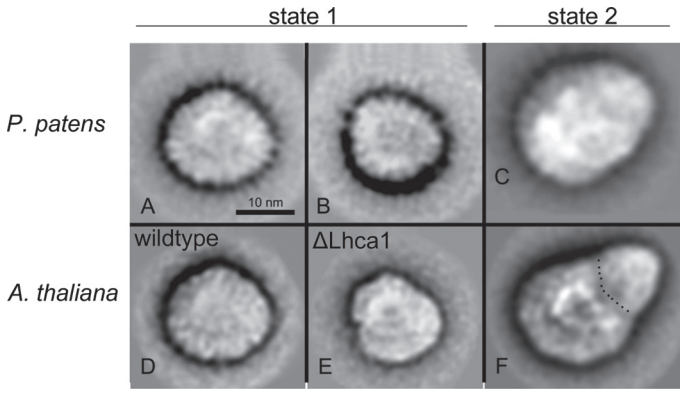

Fig. 4. Transmission electron microscopy and single-particle analysis of the isolated PSI–LHCI complex of *Physcomitrella*. Projection maps of PSI from *Physcomitrella* in state 1 summed from 921 particles (A) and from 395 particles (B), and in state 2 summed from 613 (C), in comparison with *Arabidopsis* PSI maps from state 1 (D, E) and from state 2 (F). The dotted line indicates the border between the core part and the extra antenna moiety attached under state 2. Parts (D) and (E) have been reproduced from Wientjes *et al.* (2009); part (F) was reproduced from Galka *et al.* (2012).

Topology of the PSI–LHCI complex

Based on the higher mobility of isolated the PSI–LHCI complex on native gels, it was suggested by earlier studies that the PSI–LHCI complex of *Physcomitrella* is smaller than that of *Arabidopsis* and *Chlamydomonas* (Alboresi *et al.*, 2008). This might reflect the absence of the Lhca4 in *Physcomitrella*, which in turn leads to a smaller LHCI complex. However, to date, no further evidence has been presented on this matter. Therefore, purified and homogeneous preparations of PSI–LHCI complexes of *Physcomitrella* were analysed using transmission electron microscopy and single-particle analysis. Classification of single-particle projection maps resulted in two maps of different size, indicating that the PSI–LHCI complex is present in two forms differing in size (Fig. 4A, B), with larger complex as the dominant form with a ratio of ~3:1. This larger projection map (Fig. 4A) stemmed from 921 particles, and although these particles lacked a distinct outline and features making them hard to align, they resembled the structure of PSI–LHCI complexes isolated from wild-type *Arabidopsis* (Fig. 4D) (Wientjes *et al.*, 2009). The smaller projection (Fig. 4B) represented a sum of only 395 top projections and hence the image resolution was low. However, it is important to note that these smaller projections were found repeatedly in different independent biological and technical replicates.

When analysing PSI–LHCI particles isolated from state 2, an additional density in the PSI–LHCI complex became evident, and a sum of 613 projections is shown in Fig. 4C. This projection looked very similar to PSI–LHCI–LHCII complexes isolated from higher plants under state 2 (Fig. 4F) (Kouril *et al.*, 2005; Wientjes *et al.*, 2009). This indicated that, under state 2 conditions, additional LHCII proteins attach to PSI in *Physcomitrella*, supporting the results obtained with chlorophyll *a* fluorescence measurements.

Discussion

Subunit composition of the moss PSI–LHCI complex

Intact PSI–LHCI complexes were isolated from *Physcomitrella* and its subunit composition was studied in detail. It was evident that the evolutionary intermediate position of *Physcomitrellas* is also reflected in the subunit composition of the PSI core. While still retaining the cyanobacterial PsaM subunits, it also contains the plant-specific PsaG, -H, and -O subunits. However, a PsaN homologue could not be identified (Table 1). In addition, the protein sequence of PsaF is an example that *Physcomitrella* still retains a more ancient version of a protein compared with higher plants. *Physcomitrella* PsaF still contains a 7 aa C-terminal extension, which can also be found in cyanobacteria and in red and green algae but not in higher plants (Supplementary Fig. S2). This extension has been proposed to be involved in the interaction with phycobilisomes (Vanselow *et al.*, 2009); however, due to the fact that it is still present in green algae and moss, which do not possess phycobilisomes, the extension might serve a different purpose.

For all of the nuclear-encoded PSI core subunits, as well as for the light-harvesting proteins, *Physcomitrella* encodes numerous isoforms (Table 1) (Alboresi *et al.*, 2008). Interestingly, this diversity could also be detected at the protein level within native PSI–LHCI complexes (Table 1 and Supplementary Table S1). This striking wealth of isoforms raises the question of their biological significance.

Molecular heterogeneity of PSI and the presence of two isoforms for PsaD, -E, and -H is well known in higher plants such as *Nicotiana* and *Arabidopsis* (Obokata *et al.*, 1993; Jensen *et al.*, 2007). In *Nicotiana sylvestris*, which encodes two PsaD isoforms, a differential expression pattern during leaf development has been shown. While the PsaD-1 level is highest in developing leaves, the PsaD-2 protein level peaks in mature leaves (Yamamoto *et al.*, 1993). In *Arabidopsis*, PsaD-1 has been shown to be the dominating form; however, it can be functionally replaced by overexpressing the almost identical PsaD-2 isoform (Ihnatowicz *et al.*, 2004). To date, no distinct function has been attributed to either of the PsaD isoforms. It has been speculated that duplicated genes have been retained to allow the same subunits to respond to multiple signal transduction pathways (Ihnatowicz *et al.*, 2004).

Physcomitrella underwent whole-genome duplication approximately 45 million years ago, leading to a wealth of multiple genes (Rensing *et al.*, 2007). One effect of gene duplication is that it alleviates the pressure to maintain a single important gene, introducing the potential for development of new genes. It is tempting to speculate that *Physcomitrella* retained the high number of isoforms and specialized them to fine-tune the structure and function of PSI during different developmental stages or stress conditions. Expression data from GENEVESTIGATOR (http://www.genevestigator.com) indicated an isoform-specific gene regulation

during development (Supplementary Fig. S5 at *JXB* online). For example, the PsaD and PsaL isoforms show differential expression during the different development stages. Also, for the isoforms of PsaF, we could see differences in expression pattern based on EST data. PpPsaF-3 is the dominating form in the gametophore while being only the third most abundant form in the protonemal stage (Table 1). However, it remains to be shown experimentally that the different isoforms have a distinct functional role.

Structure of the PSI–LHCI complex

Based on native gel electrophoresis, it has been proposed previously that the PSI–LHCI complex of *Physcomitrella* is smaller than its plant counterpart (Alboresi *et al.*, 2008). Our data obtained by electron micrscopy imaging analysis of isolated PSI particles did not support these findings. Interestingly, we found two populations of PSI complexes. The larger particles (Fig. 4A), which were present in the majority, represented a PSI with four Lhca proteins at the PsaF/PsaJ side of the PSI core, as seen in higher plants (Fig. 4D) (Boekema *et al.*, 2001; Ben-Shem *et al.*, 2003). This raises the question of which Lhca protein is replacing Lhca4 in the complex, as *Physcomitrella* does not have an Lhca4 homologue (Alboresi *et al.*, 2008).

It has been shown in *Arabidopsis* that deletion of an Lhca protein leads to a hole in the PSI–LHCI complex, as each individual Lhca protein has a fixed position (Ballottari *et al.*, 2007; Wientjes *et al.*, 2009). However, for Lhca4, a notable exception was found. In ΔLhca4 plants (Fig. 4E), a small fraction of complete complex containing four Lhca proteins could be isolated. Further analysis suggested that Lhca5 occupies the Lhca4 position, thereby forming a complete complex (Wientjes *et al.*, 2009). One could envision a similar scenario in *Physcomitrella*. However, semi-quantitative analysis of our proteomics data revealed that the Lhca5 protein level was much lower than that of Lhca1, -2, and -3, which are present in a nearly 1:1:1 stoichiometry (Supplementary Fig. S6 at *JXB* online). This was further supported by a preliminary analysis of transcript level derived from RNAseq data of *Physcomitrella* (Supplementary Fig. S7 at *JXB* online). Also here Lhca5 showed a much lower expression compared with the other Lhca proteins. Hence, one of the Lhca1–Lhca3 isoforms has to occupy the Lhca4 position in order to form the half-moon-shaped LHCI complex. However, which of the Lhca proteins undertakes this remains to be elucidated in a future study.

It is of note that we were able to find two different sizes of PSI particles in *Physcomitrella* (Fig. 4A, B). Given the fact that we found this size distribution in numerous independent PSI preparations and that smaller PSI particles have been reported previously (Alboresi *et al.*, 2008), it is unlikely that these different sizes are mere preparation artefacts. It is possible that the two forms represent a dynamic equilibrium that responds to different light intensities or qualities. The analysis is further complicated by the fact that PSI does not possess distinct outlines, which makes it technically challenging to obtain high-quality images. In contrast, for PSII–LHCII particles, which have a much more distinct outline, only a few images are necessary to obtain good-quality pictures (Supplementary Fig. S8 at *JXB* online).

Function of the PSI–LHCI complex

As *Physcomitrella* also encodes cyt$_{c6}$, which could potentially be an alternative electron donor to PSI, we tested this possibility in an *in vitro* NADP$^+$ photoreduction assay. However, under the assay conditions used, it was clear that *Physcomitrella* was not able to accept electrons from cyt$_{c6}$ (Table 2), showing a similar behaviour to that of *Arabidopsis*. It should be noted that the cyt$_{c6}$ used efficiently donates electrons to cyanobacterial PSI (data not shown). It has been proposed previously that, while cyt$_{c6}$ can serve as an electron donor in green algae such as *Chlamydomonas*, it has acquired novel functions not related to electron transport to PSI throughout the evolution of higher plants (Weigel *et al.*, 2003). Following this idea, we analysed the phylogeny of different cyt$_{c6}$ sequences including the one from *Physcomitrella* (Supplementary Fig. S9 at *JXB* online). Clearly, the *Physcomitrella* cyt$_{c6}$ sequence grouped with the cyt$_{c6}$ of higher plants, indicating that already in moss cyt$_{c6}$ has acquired a novel function.

With respect to state transition, we showed that *Physcomitrella* is able to perform state transitions. However, based on the state transition coefficient we obtained [(Fm1 – Fm2)/Fm2] (Jensen *et al.*, 2000), it appeared that the movement of the PSII antenna towards PSI happens to a smaller extent than in *Arabidopsis* under the same conditions. Recently, Lhcb9, a light-harvesting protein that associates with PSII, was characterized in *Physcomitrella* (Alboresi *et al.*, 2011). This Lhcb9 protein, unlike all other known LHCII protein, harbours a red-shifted chlorophyll leading to changes in absorption properties of PSII. Hence, the excitation pressure on PSII in *Physcomitrella* might be different from that in *Arabidopsis* under the state 2 light-inducing conditions we applied in our experiments.

Supplementary data

Supplementary data are available at *JXB* online.

Supplementary Fig. S1. Sequence comparison of PsaD isoforms of *Physcomitrella*.

Supplementary Fig. S2. Alignment of full-length PsaF proteins from different species.

Supplementary Fig. S3. Alignment of the three different isoforms of PsaK of *Phscomitrella*.

Supplementary Fig. S4. Traces from the state transition experiment.

Supplementary Fig. S5. Expression data from GENEVESTIGATOR for selected isoforms.

Supplementary Fig. S6. Label-free quantification of PSI-LHCI proteins in *Physcomitrella*.

Supplementary Fig. S7. Expression profile of light-harvesting proteins in *Physcomitrella*.

Supplementary Fig. S8. Transmission electron microscopy and single-particle analysis of isolated PSII–LHCII complexes of *Physcomitrella*.

Supplementary Fig. S9. Phylogenetic tree based on the protein sequence of cytochrome c6 sequences.

Supplementary Table S1. Identified proteins and corresponding peptides.

Supplementary Table S2. Photosynthetic parameters derived from chlorophyll *a* fluorescence measurements.

Acknowledgements

The authors gratefully acknowledge financial support from the Villum Foundation to the research centre 'Pro-Active Plants', from the 'Center of Synthetic Biology' funded by the UNIK research initiative of the Danish Ministry of Science (09-064047), and from the 'Nutriefficient' project (10-093498) funded by the Danish Strategic Research Council. A.B. is grateful for support from the Deutsche Forschungsgemeinschaft (BU2563/1-1).

References

Alboresi A, Caffarri S, Nogue F, Bassi R, Morosinotto T. 2008. In silico and biochemical analysis of *Physcomitrella patens* photosynthetic antenna: identification of subunits which evolved upon land adaptation. *PLoS One* **3,** e2033.

Alboresi A, Gerotto C, Cazzaniga S, Bassi R, Morosinotto T. 2011. A red-shifted antenna protein associated with photosystem II in *Physcomitrella patens*. *Journal of Biological Chemistry* **286,** 28978–28987.

Alboresi A, Gerotto C, Giacometti GM, Bassi R, Morosinotto T. 2010. *Physcomitrella patens* mutants affected on heat dissipation clarify the evolution of photoprotection mechanisms upon land colonization. *Proceedings of the National Academy of Sciences U S A* **107,** 11128–11133.

Amunts A, Nelson N. 2009. Plant photosystem I design in the light of evolution. *Structure* **17,** 637–650.

Ashton NW, Cove DJ. 1977. Isolation and preliminary characterization of auxotrophic and analog resistant mutants of moss, *Physcomitrella patens*. *Molecular & General Genetics* **154,** 87–95.

Ashton NW, Grimsley NH, Cove DJ. 1979. Analysis of gametophytic development in the moss, *Physcomitrella patens*, using auxin and cytokinin resistant mutants. *Planta* **144,** 427–435.

Ballottari M, Dall'Osto L, Morosinotto T, Bassi R. 2007. Contrasting behavior of higher plant photosystem I and II antenna systems during acclimation. *Journal of Biological Chemistry* **282,** 8947–8958.

Ben-Shem A, Frolow F, Nelson N. 2003. Crystal structure of plant photosystem I. *Nature* **426,** 630–635.

Boekema EJ, Jensen PE, Schlodder E, van Breemen JF, van Roon H, Scheller HV, Dekker JP. 2001. Green plant photosystem I binds light-harvesting complex I on one side of the complex. *Biochemistry* **40,** 1029–1036.

Boekema EJ, Van Roon H, Van Breemen JF, Dekker JP. 1999. Supramolecular organization of photosystem II and its light-harvesting antenna in partially solubilized photosystem II membranes. *European Journal of Biochemistry* **266,** 444–452.

Busch A, Hippler M. 2011. The structure and function of eukaryotic photosystem I. *Biochimica et Biophysica Acta* **1807,** 864–877.

Chua NH, Bennoun P. 1975. Thylakoid membrane polypeptides of *Chlamydomonas reinhardtii*: wild-type and mutant strains deficient in photosystem II reaction center. *Proceedings of the National Academy of Sciences U S A* **72,** 2175–2179.

Emanuelsson O, Nielsen H, von Heijne G. 1999. ChloroP, a neural network-based method for predicting chloroplast transit peptides and their cleavage sites. *Protein Science* **8,** 978–984.

Falkowski PG. 2006. Evolution. Tracing oxygen's imprint on earth's metabolic evolution. *Science* **311,** 1724–1725.

Frank W, Ratnadewi D, Reski R. 2005. *Physcomitrella patens* is highly tolerant against drought, salt and osmotic stress. *Planta* **220,** 384–394.

Galka P, Santabarbara S, Khuong TT, Degand H, Morsomme P, Jennings RC, Boekema EJ, Caffarri S. 2012. Functional analyses of the plant photosystem I–light-harvesting complex II supercomplex reveal that light-harvesting complex II loosely bound to photosystem II is a very efficient antenna for photosystem I in state II. *Plant Cell* **24,** 2963–2978.

Ganeteg U, Klimmek F, Jansson S. 2004. Lhca5—an LHC-type protein associated with photosystem I. *Plant Molecular Biology* **54,** 641–651.

Gerotto C, Alboresi A, Giacometti GM, Bassi R, Morosinotto T. 2011. Role of PSBS and LHCSR in *Physcomitrella patens* acclimation to high light and low temperature. *Plant, Cell & Environment* **34,** 922–932.

Haldrup A, Jensen PE, Lunde C, Scheller HV. 2001. Balance of power: a view of the mechanism of photosynthetic state transitions. *Trends in Plant Science* **6,** 301–305.

Haldrup A, Naver H, Scheller HV. 1999. The interaction between plastocyanin and photosystem I is inefficient in transgenic *Arabidopsis* plants lacking the PSI-N subunit of photosystem I. *The Plant Journal* **17,** 689–698.

Hiyama T, Ke B. 1972. Difference spectra and extinction coefficients of P700. *Biochimica et Biophysica Acta* **267,** 160–171.

Hofmann AH, Codon AC, Ivascu C, Russo VE, Knight C, Cove D, Schaefer DG, Chakhparonian M, Zryd JP. 1999. A specific member of the Cab multigene family can be efficiently targeted and disrupted in the moss *Physcomitrella patens*. *Molecular and General Genetics* **261,** 92–99.

Ihnatowicz A, Pesaresi P, Varotto C, Richly E, Schneider A, Jahns P, Salamini F, Leister D. 2004. Mutants for photosystem I subunit D of *Arabidopsis thaliana*: effects on photosynthesis, photosystem I stability and expression of nuclear genes for chloroplast functions. *The Plant Journal* **37,** 839–852.

Jansson S. 1999. A guide to the Lhc genes and their relatives in *Arabidopsis*. *Trends in Plant Science* **4,** 236–240.

Jensen K, Jensen PE, Moller BL. 2011. Light-driven cytochrome p450 hydroxylations. *ACS Chemical Biology* **6,** 533–539.

Jensen ON, Larsen MR, Roepstorff P. 1998. Mass spectrometric identification and microcharacterization of proteins from electrophoretic gels: strategies and applications. *Proteins: Structure, Function, and Bioinformatics* **33** (Suppl. 2**),** 74–89.

Jensen PE, Bassi R, Boekema EJ, Dekker JP, Jansson S, Leister D, Robinson C, Scheller HV. 2007. Structure, function and regulation of plant photosystem I. *Biochimica et Biophysica Acta* **1767,** 335–352.

Jensen PE, Gilpin M, Knoetzel J, Scheller HV. 2000. The PSI-K subunit of photosystem I is involved in the interaction between light-harvesting complex I and the photosystem I reaction center core. *Journal of Biological Chemistry* **275,** 24701–24708.

Jensen PE, Rosgaard L, Knoetzel J, Scheller HV. 2002. Photosystem I activity is increased in the absence of the PSI-G subunit. *Journal of Biological Chemistry* **277,** 2798–2803.

Klimmek F, Sjodin A, Noutsos C, Leister D, Jansson S. 2006. Abundantly and rarely expressed Lhc protein genes exhibit distinct regulation patterns in plants. *Plant Physiology* **140,** 793–804.

Kouril R, Zygadlo A, Arteni AA, de Wit CD, Dekker JP, Jensen PE, Scheller HV, Boekema EJ. 2005. Structural characterization of a complex of photosystem I and light-harvesting complex II of *Arabidopsis thaliana*. *Biochemistry* **44,** 10935–10940.

Koziol AG, Borza T, Ishida K, Keeling P, Lee RW, Durnford DG. 2007. Tracing the evolution of the light-harvesting antennae in chlorophyll *a/b*-containing organisms. *Plant Physiology* **143,** 1802–1816.

Lichtenthaler HK. 1987. Chlorophylls and carotenoids—pigments of photosynthetic biomembranes. *Methods in Enzymology* **148,** 350–382.

Markwell JP, Thornber JP, Skrdla MP. 1980. Effect of detergents on the reliability of a chemical assay for P-700. *Biochimica et Biophysica Acta* **591,** 391–399.

Mullet JE, Burke JJ, Arntzen CJ. 1980. Chlorophyll proteins of photosystem I. *Plant Physiology* **65,** 814–822.

Obokata J, Mikami K, Hayashida N, Nakamura M, Sugiura M. 1993. Molecular heterogeneity of photosystem I. *psaD*, *psaE*, *psaF*, *psaH*, and *psaL* are all present in isoforms in *Nicotiana* spp. *Plant Physiology* **102,** 1259–1267.

Oostergetel GT, Keegstra W, Brisson A. 1998. Automation of specimen selection and data acquisition for protein electron crystallography. *Ultramicroscopy* **74,** 47–59.

Peers G, Truong TB, Ostendorf E, Busch A, Elrad D, Grossman AR, Hippler M, Niyogi KK. 2009. An ancient light-harvesting protein is critical for the regulation of algal photosynthesis. *Nature* **462,** 518–521.

Peng L, Shikanai T. 2011. Supercomplex formation with photosystem I is required for the stabilization of the chloroplast NADH dehydrogenase-like complex in *Arabidopsis*. *Plant Physiology* **155,** 1629–1639.

Rensing S, Ick J, Fawcett J, Lang D, Zimmer A, Van de Peer Y, Reski R. 2007. An ancient genome duplication contributed to the abundance of metabolic genes in the moss *Physcomitrella patens*. *BMC Evolutionary Biology* **7,** 130.

Rintamaki E, Martinsuo P, Pursiheimo S, Aro EM. 2000. Cooperative regulation of light-harvesting complex II phosphorylation via the plastoquinol and ferredoxin-thioredoxin system in chloroplasts. *Proceedings of the National Academy of Sciences U S A* **97,** 11644–11649.

Sonoike K, Katoh S. 1988. Effects of sodium dodecyl sulfate and methyl viologen on the differential extinction coefficient of P-700—a band shift of chlorophyll *a* associated with oxidation of P-700. *Biochimica et Biophysica Acta (BBA)—Bioenergetics* **935,** 61–71.

Turkina MV, Kargul J, Blanco-Rivero A, Villarejo A, Barber J, Vener AV. 2006. Environmentally modulated phosphoproteome of photosynthetic membranes in the green alga *Chlamydomonas reinhardtii*. *Molecular & Cellular Proteomics* **5,** 1412–1425.

Vanselow C, Weber AP, Krause K, Fromme P. 2009. Genetic analysis of the Photosystem I subunits from the red alga, *Galdieria sulphuraria*. *Biochimica et Biophysica Acta* **1787,** 46–59.

Weigel M, Varotto C, Pesaresi P, Finazzi G, Rappaport F, Salamini F, Leister D. 2003. Plastocyanin is indispensable for photosynthetic electron flow in *Arabidopsis thaliana*. *Journal of Biological Chemistry* **278,** 31286–31289.

Wientjes E, Oostergetel GT, Jansson S, Boekema EJ, Croce R. 2009. The role of Lhca complexes in the supramolecular organization of higher plant photosystem I. *Journal of Biological Chemistry* **284,** 7803–7810.

Wolf L, Rizzini L, Stracke R, Ulm R, Rensing SA. 2010. The molecular and physiological responses of *Physcomitrella patens* to ultraviolet-B radiation. *Plant Physiology* **153,** 1123–1134.

Wood PM. 1978. Interchangeable copper and iron proteins in algal photosynthesis. Studies on plastocyanin and cytochrome c-552 in *Chlamydomonas*. *European Journal of Biochemistry* **87,** 9–19.

Yamamoto Y, Tsuji H, Obokata J. 1993. Structure and expression of a nuclear gene for the Psi-D subunit of Photosystem-I in *Nicotiana sylvestris*. *Plant Molecular Biology* **22,** 985–994.